8-1-2024

Piecewise fractional derivatives and wavelets in epidemic modeling

Mutaz Mohammad
Zayed University, mutaz.mohammad@zu.ac.ae

Mohyeedden Sweidan
Concord University

Alexander Trounev
Kuban State Agrarian University

Alexandria Engineering Journal 101 (2024) 245–253

Contents lists available at ScienceDirect

Alexandria Engineering Journal

journal homepage: www.elsevier.com/locate/aej

Original article

Piecewise fractional derivatives and wavelets in epidemic modeling

Mutaz Mohammad [a,*], Mohyeedden Sweidan [b], Alexander Trounev [c]

[a] Zayed University, Abu Dhabi, UAE
[b] Concord University, Athens, WV, United States of America
[c] Kuban State Agrarian University, Krasnodar, Russia

ARTICLE INFO

Keywords:
Piecewise differentiation
Bernoulli wavelets
Fractional derivatives
Collocation techniques
Epidemiological modeling
Numerical simulations

ABSTRACT

In this paper, we propose a novel methodology for studying the dynamics of epidemic spread, focusing on the utilization of fundamental mathematical concepts related to piecewise differential and integral operators. These mathematical tools play a crucial role in the process of modeling epidemic phenomena, enabling us to investigate the behavior of infectious diseases within defined time intervals. Our primary objective is to enhance our understanding of epidemic dynamics and the underlying influencing factors. We introduce the Susceptible–Infectious–Recovered (SIR) model as the foundational framework, which is formulated as a system of differential equations. Our approach involves discretizing time and employing interpolation techniques for integrals, specifically utilizing the collocation method with Bernoulli wavelets. By incorporating piecewise derivatives, we are able to conduct comprehensive simulations and analyses of epidemic spread under various intervention strategies, including social distancing measures. The outcomes of our numerical simulations serve to validate the efficacy of our proposed methodology, offering valuable insights into the intricate dynamics of real-world epidemic scenarios. This contribution significantly advances the field of epidemic control optimization, providing an integrated framework that seamlessly integrates fractional calculus, piecewise differential derivatives, and the capabilities of wavelets. Our findings provide crucial guidance for policymakers and healthcare leaders, offering a deeper understanding of the effectiveness of different control strategies. By considering our innovative approach, we can better inform and shape epidemic control measures, ultimately enhancing public health and fortifying our defenses against infectious diseases.

1. Introduction

Mathematical models play a crucial role in understanding and addressing emerging global issues, such as disease transmission, recovery, and mortality. In epidemiology, mathematical models are used to explore the underlying factors that affect disease transmission and suggest potential control measures. However, modeling real-world data can be challenging due to variations, small sample sizes, or measurement errors [1]. Striking a balance between simplicity and detail in these models requires careful consideration of trade-offs between highlighting general qualitative behavior and generating specific quantitative predictions.

One of the most extensively studied models in infectious disease dynamics is the susceptible–infected–recovered (SIR) model, renowned for its realistic portrayal of disease spread dynamics. The SIR model operates on the premise that populations can exist in one of three states: susceptible, infected, or recovered (removed) [2,3]. It relies on two fundamental assumptions: infected individuals transmit the disease to susceptible individuals at a rate proportional to the number of infected individuals, and infected individuals recover at a constant rate. Amid the ongoing global pandemic, diverse strategies have been implemented worldwide to curb infection spread, including social distancing, lockdowns, and quarantines, among others [4–12]. In this paper, we propose a novel approach to optimize the control strategy of the SIR epidemic model within specified time constraints. We utilize a collocation technique based on Bernoulli wavelets to tackle the optimization problem and conduct numerical experiments. Our methodology encompasses three distinct cost functionals and determines the optimal duration of lockdown periods.

Traditionally, the optimization of the SIR epidemic model has involved Pontryagin's Minimum Principle [13], constrained by finite control resources and appropriate cost functions [14–16], coupled with various numerical techniques [17–19]. However, our proposed method introduces an innovative approach by harnessing the potential of Bernoulli wavelets [20]. These wavelets, particularly suitable for machine learning applications, not only enhance numerical accuracy but also pave the way for future advancements in epidemic control

* Corresponding author.
E-mail address: Mutaz.Mohammad@zu.ac.ae (M. Mohammad).

https://doi.org/10.1016/j.aej.2024.05.053
Received 20 September 2023; Received in revised form 28 March 2024; Accepted 17 May 2024
Available online 31 May 2024

optimization, utilizing our AI-based algorithm [21]. Moreover, recent literature has presented diverse classes of local differential and integral operators, each serving specific purposes and theoretical properties. In our study, we adopt a form of a system of piecewise fractional differential equations, as outlined in Section 3.1, to address certain epidemic dynamics, particularly in the context of the Zika virus model.

Epidemic modeling aims to understand and predict the spread of infectious diseases within populations. One of the fundamental challenges in this field is capturing the complex dynamics of disease transmission, which often exhibit non-linear and time-varying behavior. Traditional mathematical models, such as those based on ordinary differential equations (ODEs), may struggle to accurately represent certain aspects of epidemic spread, particularly when confronted with discontinuities or abrupt changes in transmission rates, intervention strategies, or population dynamics. Piecewise differential and integral operators offer a powerful mathematical framework for addressing these challenges in epidemic modeling. Unlike classical derivatives, which assume continuous and smooth changes in system variables, piecewise derivatives allow for the modeling of discontinuous or piecewise continuous functions. This flexibility enables researchers to capture various phenomena observed in real-world epidemics, such as the sudden implementation of control measures (e.g., quarantine or social distancing), fluctuations in transmission rates due to seasonal changes or behavioral factors, and the emergence of localized outbreaks or superspreading events. By incorporating piecewise derivatives into epidemic models, researchers can more accurately simulate the dynamics of infectious diseases and assess the effectiveness of different control strategies. For example, piecewise differential equations can be used to model the temporal evolution of disease compartments (e.g., susceptible, infectious, and recovered individuals) within defined time intervals, allowing for the analysis of epidemic behavior over discrete time steps. Piecewise integral operators, on the other hand, enable the calculation of cumulative effects, such as the total number of infections or the impact of interventions on disease transmission, over finite time intervals. The utility of piecewise derivatives extends beyond epidemic modeling to various other fields, including ecology, finance, and engineering. In epidemiology, piecewise models have been applied to study a wide range of infectious diseases, including influenza, HIV/AIDS, and COVID-19, providing valuable insights into the dynamics of disease spread and informing public health policies and interventions.

In summary, our study introduces a novel methodology for studying epidemic spread dynamics, focusing on the utilization of fundamental mathematical concepts such as piecewise differential and integral operators. The main contribution of our research lies in the development of a comprehensive framework that integrates advanced mathematical tools with the SIR model, enabling detailed simulations and analyses of epidemic phenomena within defined time intervals. By considering concepts from fractional calculus, piecewise differential derivatives, and wavelets, our approach offers a fresh perspective on epidemic control optimization, paving the way for more accurate and efficient strategies in disease management. Furthermore, we propose a novel application of the collocation method with Bernoulli wavelets for optimizing control strategies within the SIR model framework, providing enhanced numerical accuracy and efficiency. Through our study, we aim to enhance our understanding of epidemic dynamics, optimize control strategies, and provide valuable guidance for policymakers and healthcare leaders in addressing current challenges in epidemic control optimization. Overall, the incorporation of piecewise derivatives into epidemic modeling represents a significant advancement in our ability to understand and control infectious diseases. By capturing the complex and dynamic nature of epidemic phenomena, piecewise models offer researchers a more comprehensive and accurate tool for studying disease transmission and developing effective strategies for epidemic control and prevention.

2. The SIR model and numerical algorithm

The SIR model with control function through social distancing $u(t)$ and cost function $f(x,u)$ can be expressed as follows (see [16]):

$$\frac{ds}{dt} = -s(t)(\beta - u(t))x(t), \tag{1}$$

$$\frac{dx}{dt} = s(t)(\beta - u(t))x(t) - \gamma x(t), \tag{2}$$

$$\frac{dy}{dt} = f(x,u), \tag{3}$$

defined on the interval $[0,T]$ with the initial conditions $s(0) = s_0$, $x(0) = x_0$, $y(0) = 0$. Here, f, β, T, and γ are given parameters, s represents the density of susceptible population, x denotes the density of infected population of various kinds, and y represents the recovered population (the cost functional to be minimized). These cost functionals are introduced to quantify the mortality rate over time.

We have employed various scenarios to assess whether different cost functionals can result in optimal control. Thus, we are examining the incremental change in the susceptible population while adjusting the fluctuations in the infected population according to the chosen cost function.

In our notation, $s(t)$ represents the portion of the population that is healthy but vulnerable to the disease at time t, while $x(t)$ denotes the portion of the population that is infected. According to the SIR model, the number of individuals infected by a single infected person is directly linked to the proportion of the population $s(t)$ that remains susceptible to the disease.

The function to be minimized is denoted as $y(t_f,u)$, or equivalently represented as the integral

$$\int_0^{t_f} f(x,u)dx.$$

In accordance with Refs. [14,19], we assume the following parameters and initial data for the model (1)–(3):

$$\beta = 0.16, \gamma = 0.06, s_0 = 0.999, x_0 = 0.001, t_f = 360\ days,\ \ s_0 + x_0 \le 1.$$

We have chosen these parameters following the framework outlined in Ref. [16] to offer insights for policymaking and epidemic management. For example, we have calibrated the parameters to mirror the dynamics observed during the COVID-19 pandemic. Assuming an average infection duration of 18 days, we set $\gamma = 0.06$ $(= 1/18)$. The coefficients $\beta = 0.16$ and the initial conditions $x_0 = 0.001, s_0 = 0.999$ were determined in line with findings from Refs. [14,19]. These studies suggest that commonly used parameters for modeling COVID-19 transmission advocate for an optimal strategy entailing immediate implementation of social distancing measures, resulting in a 60% reduction in transmission rates, sustained over approximately 360 days.

The Reproduction Number: We adhere to standard epidemiological terminology and define the basic reproduction rate R_0 of the disease as the number of individuals a single infected person would infect when they are the sole carrier of the disease, with transmission at its peak, represented as $R_0 = \beta/\gamma$. R_0 quantifies the speed at which the disease would spread in the absence of interventions, while $R(t) = \gamma^{-1}\beta(t) \times s(t)$ quantifies the rate of disease spread at time t, given the strategy implemented by the planner and the current proportion of the susceptible population. In our model, we estimate R_0 to be approximately 2.7 (calculated as 0.16/0.06).

There are three cost functionals tested with model (1)–(3). The first is quadratic in both state and control, given by

$$f = x^2 + u^2. \tag{4}$$

The second is quadratic in state and linear in control, expressed as

$$f = 30x^2 + u. \tag{5}$$

The third cost functional is linear in both state and control, represented as

$$f = 20x + u. \tag{6}$$

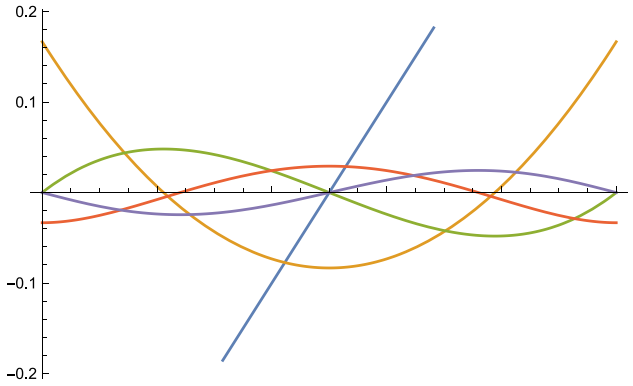

Fig. 1. The graphs of B_n, for $n = 1, \ldots, 5$.

A common approach to define the control function in a social distancing scenario is to set $u = 0$ during the no-control period t_n and $u = u_0 > 0$ during the lock-down period t_l. For simplicity, we assume $t_n = nt_c$ and $t_l = lt_c$, where n and l are integers and t_c is the minimum time period for implementing the social distancing policy.

With this control function definition, the optimization problem aims to find the minimum value among the set of $y(t_f, u_i)$, where i ranges from 1 to N. The value of N can be approximated as $2^{t_f/t_c}$, where t_f is the final time of the simulation.

To solve this optimization problem, we employ the collocation method, utilizing Bernoulli wavelets. Fig. 1 presents several graphs of Bernoulli polynomials, essential in the collocation method.

The piecewise function $p_{1,2}(x)$ is defined as follows:

$$p_{1,2}(x) = \begin{cases} B_{1,2}(x) & 0 \le x \le 1 \\ 0 & \text{otherwise,} \end{cases}$$

where $B_{1,2}$ represent the Bernoulli polynomials given by

$$B_1 = -\frac{1}{2} + x, B_2 = \frac{1}{6} - x + x^2.$$

Define the wavelets based on indices j and k as follows:

$$\psi_1(j,k,x) = p_1(xj - k)$$
$$\psi_2(j,k,x) = p_2(xj - k)$$
$$\psi(j,k,x) = \frac{1}{2}(\psi_1(j,k,x) + \psi_2(j,k,x))$$

Then, let us define a vector Ψ of length $M = 2^{n+1}$, where $n = 1, 2, \ldots$, representing the number of collocation points:

$$\Psi = \left(1, \psi(1,0,x), \ldots, \psi(2^j,k,x), \psi(2^n, 2^{n-1}, x)\right)$$
$$j = 0, 1, 2, \ldots, n; \quad k = 0, 1, 2, \ldots, 2^{j-1}$$

Finally, we define the integral of vector Ψ as follows:

$$\Psi_I = \int_0^x \Psi(x), dx$$
$$= \left(x, \psi_I(1,0,x), \ldots, \psi_I(2^j,k,x), \psi_I(2^n, 2^{n-1}, x)\right)$$

where $j = 0, 1, 2, \ldots, n$ and $k = 0, 1, 2, \ldots, 2^{j-1}$.

Here, $\psi_I(j,k,x)$ can be defined explicitly as

$$\psi_I(j,k,x) = \begin{cases} \frac{-k + k^2}{2j} & \text{if } j > 0, k = 0, 1/j - x < 0 \\ \frac{-x + 3k^2x - 3jkx^2 + j^2x^3}{6} & \text{if } j > 0, k = 0, x > 0, 1/j - x \ge 0 \\ \frac{k - k^3 - jx + 3jk^2x - 3j^2kx^2 + j^3x^3}{6j} & \text{if } j > 0, k > 0, k/j - x < 0, \\ & 1/j + k/j - x \ge 0 \\ 0 & \text{otherwise} \end{cases}$$

With vectors Ψ and Ψ_I, we can discretize the SIR model (1)–(3) using the following steps. First, we map the solution onto the unit interval $0 \le t \le 1$ using the substitution $t = t_f t'$. Second, we define the numerical solutions as follows:

$$\dot{s} = S\Psi, \quad \dot{x} = X\Psi, \quad \dot{y} = Y\Psi, \; s \quad = S\Psi_I + c_1, \quad x = X\Psi_I + c_2,$$
$$y = Y\Psi_I + c_3,$$

where S, X, Y, and c are unknown vectors to be computed using a discrete form of (1)–(3). This implies

$$\begin{aligned} \frac{S\Psi(t_m)}{t_f} &= -(S\Psi_I(t_m) + c_1)(\beta - u(t_m))(X\Psi_I(t_m) + c_2), \\ \frac{X\Psi(t_m)}{t_f} &= (S\Psi_I(t_m) + c_1)(\beta - u(t_m))(X\Psi_I(t_m) + c_2) - \gamma X\Psi_I(t_m), \\ \frac{Y\Psi(t_m)}{t_f} &= f(X\Psi_I(t_m), u(t_m)), \end{aligned} \tag{7}$$

where t_m, $m = 1, 2, \ldots, M$, are collocation points.

To solve the system of algebraic equations (7) for a given cost functional, we employ the Newton's iterative method for each trial function u_i, where i ranges from 1 to $2^{t_f/t_c}$. In our numerical analysis, we choose $t_c = t_f/8$. Using this approach, we can compute the minimum value of $y(1, u_i)$ for a set of trial control functions u_i, where i ranges from 1 to 256.

To ensure accurate numerical solutions with an appropriate error margin, it is essential to define a minimum number of collocation points. To determine this, we initially solved the system of Eqs. (1)–(3) without control, i.e., $u = 0$, and with the cost functional (4) using the Runge–Kutta method of order 8. The resulting numerical solution was then compared to the collocation method using various numbers of collocation points, as depicted in Fig. 2. Through this comparison, we determined that a minimum of 32 collocation points was necessary. Attempting to use fewer points resulted in numerical instability due to the stiffness of the system (1)–(3), which is influenced by the small parameter $1/t_f$.

The optimization results are depicted in Figs. 2, 3, and 4, representing different scenarios with varying values of u_0 alongside their corresponding cost functionals. Each case was computed using $M = 32$ collocation points.

Fig. 3 illustrates the optimal solution for the cost functional (4) with $u_0 = 0.04$ (top line) and $u_0 = 0.08$ (bottom line). In Fig. 4, the optimal solution is presented for the cost functional (5) with $u_0 = 0.08$ (top line) and $u_0 = 0.1$ (bottom line). Lastly, Fig. 5 showcases the optimal solution for the cost functional (6) with $u_0 = 0.04$ (top line) and $u_0 = 0.06$ (bottom line).

Multiple tests were conducted with a shorter minimal duration of social distancing, set at $t_c = t_f/16$. In this scenario, 2^{16} numerical solutions of the SIR epidemic model were compared to minimize the cost functional. Fig. 6 presents the data computed with the same initial conditions, u_0, and functional as in Fig. 2, but with $t_c = 360/16$. The data computed with $u_0 = 0.08$ exhibit similarities to those in Fig. 3. However, for $u_0 = 0.04$, a new minimum and a different state emerge.

3. Applications of piecewise derivative

In this section, we present two applications of piecewise derivative models, focusing on the Zika virus and Optimal SIR models.

3.1. Zika virus model

The application of fractional differential calculus to tackle important and practical challenges has experienced significant growth recently. Readers are encouraged to explore the following references, which cover a diverse range of applications for these operators. For example, see Refs. [22–32]. In this section, we explore an application of the SIR model (1)–(3) to the simulation of a Zika virus epidemic, a

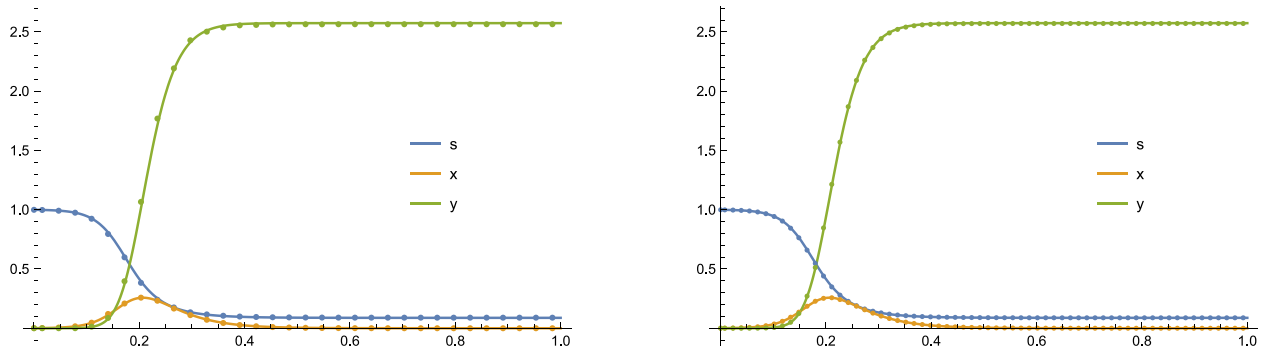

Fig. 2. Numerical solution of SIR epidemic model at $u = 0$ by the Runge–Kutta method (solid lines) and collocation method (points) with $M = 32$ (left) and $M = 64$ (right).

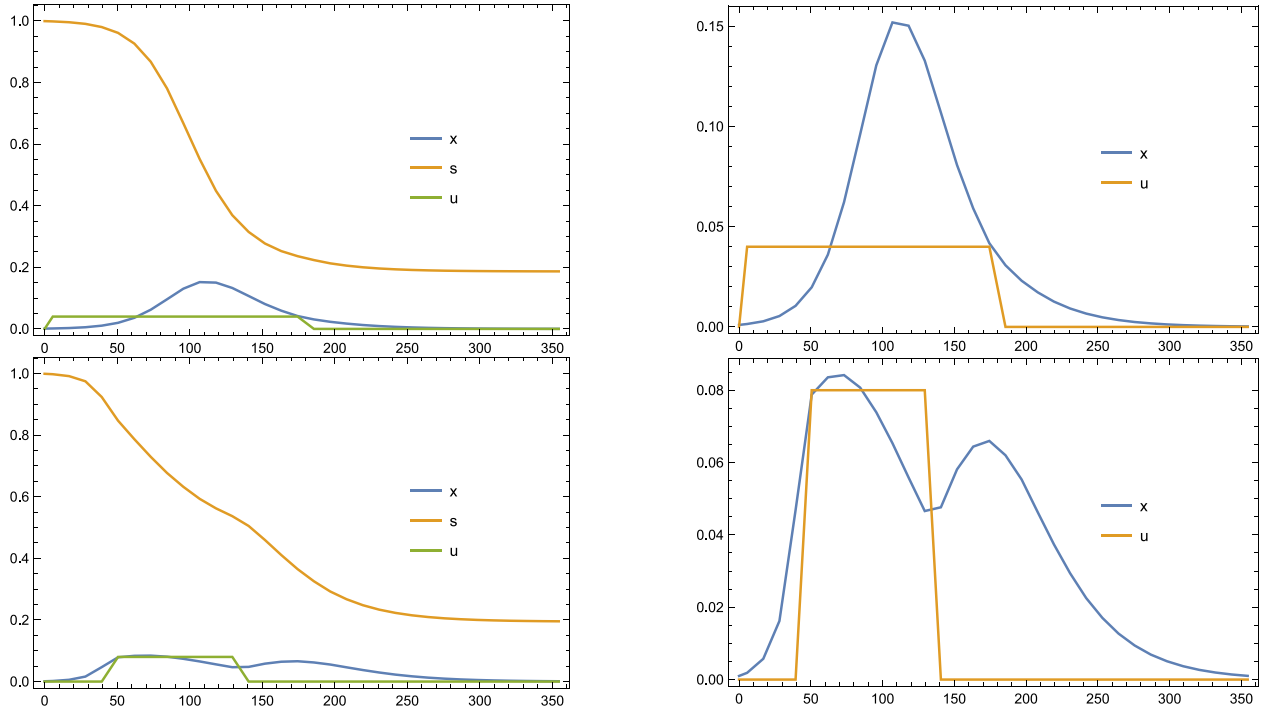

Fig. 3. Numerical optimal solution of SIR epidemic model with the cost functional (4) at $u_0 = 0.04$ (upper line), and $u_0 = 0.08$ (bottom line).

disease that can be transmitted from person to person through the blood of an infected individual. To this end, we consider an extension of the SIR model in the form of a system of piecewise fractional differential equations in [33] given by

$$\begin{aligned}
&{}_0^{PG}D_g^{\alpha}x_1 = \Lambda_h - \beta_1\gamma_1 x_1(t)x_4(t) - d_1x_1(t),\\
&{}_0^{PG}D_g^{\alpha}x_2 = \beta_1\gamma_1 x_1(t)x_4(t) - d_1x_2(t),\\
&{}_0^{PG}D_g^{\alpha}x_3 = \Lambda_m - \beta_2\gamma_2 x_2(t)x_3(t) - d_2x_3(t),\\
&{}_0^{PG}D_g^{\alpha}x_4 = \beta_2\gamma_2 x_2(t)x_3(t) - d_2x_4(t),
\end{aligned} \tag{8}$$

where ${}_0^{PG}D_g^{\alpha}$ denotes the global fractional derivative given by

$${}_0^{PC}D_g^{\alpha}f(t) = \begin{cases} f'(t) & 0 \le t \le t_1,\\ {}_0^{C}D_g^{\alpha}f(t) & t_1 \le t \le T. \end{cases} \tag{9}$$

Here, ${}_0^{C}D_g^{\alpha}$ is the classical Caputo fractional derivative, α is the fractional order, and we have the piecewise integral operator ${}_0^{PG}J_g f(t)$, defined as follows (referring to [33]):

$${}_0^{PG}J_g f(t) = \begin{cases} \int_0^t f(\tau)d\tau, & \text{for } 0 \le t \le t_1,\\ \int_{t_1}^t f(\tau)dg(\tau), & \text{for } t_1 \le t \le T. \end{cases}$$

To approximate the Caputo fractional derivative ${}_0^{C}D_g^{\alpha}$, we adopt the piecewise derivative definition proposed in [33], which reads

$${}_0^{PC}D_g^{\alpha}f(t) = \begin{cases} f'(t) & 0 \le t \le t_1,\\ \dfrac{f'(t)}{g'(t)} & t_1 \le t \le T, \end{cases}$$

where

$$g(t) = \frac{t^{2-\alpha}}{2-\alpha}$$

is a function that ensures the smoothness of the derivative and t_1 is a breakpoint at which the derivative switches from the classical form to the fractional form.

To ensure the positivity and boundedness, it is necessary to consider that on each hyperplane bounding is positive, i.e.,

$$\beta_1\gamma_1 x_1 x_4 \ge 0, \beta_2\gamma_2 x_2 x_3 \ge 0, \Lambda_h, \Lambda_m \ge 0,$$

and that if $\|f\|_\infty = \sup_t |f(t)|$, and both f and g ($g' \ne 1$) are differentiable functions, then

$$|{}_0^{PC}D_g^{\alpha}f(t)| = \begin{cases} |f'(t)| & 0 \le t \le t_1\\ \left|\dfrac{f'(t)}{g'(t)}\right| & t_1 \le t \le T \end{cases}$$

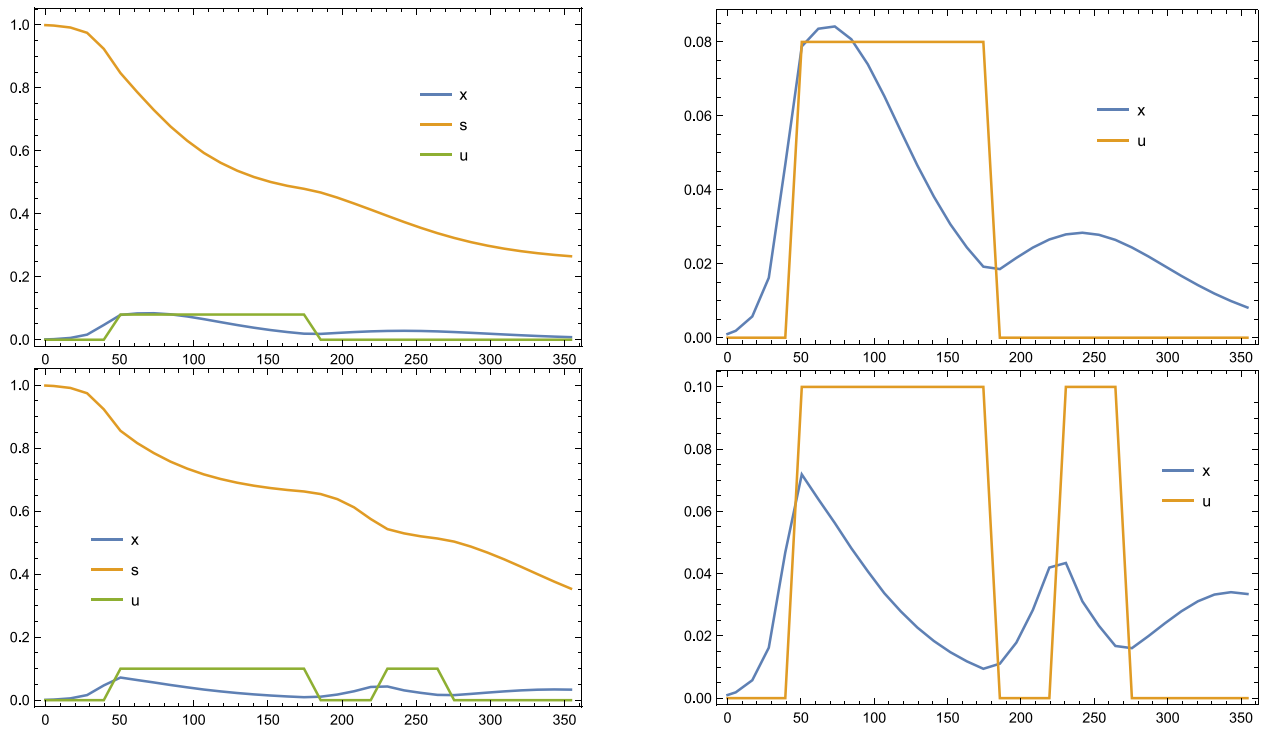

Fig. 4. Numerical optimal solution of the SIR epidemic model with the cost functional (5) for $u_0 = 0.08$ (upper Line) and $u_0 = 0.1$ (bottom Line).

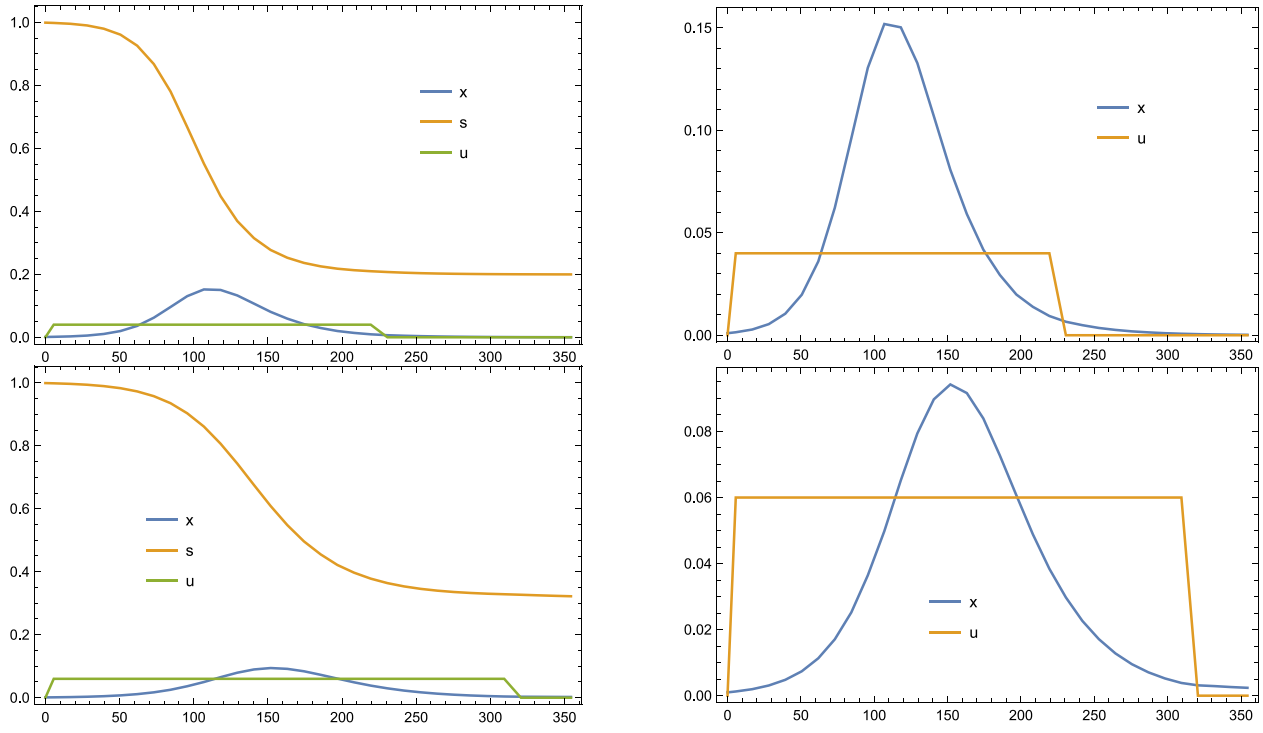

Fig. 5. Numerical optimal solution of the SIR epidemic model with the cost functional (6) for $u_0 = 0.04$ (upper Line) and $u_0 = 0.06$ (bottom Line).

$$\leq \begin{cases} \sup_{t\in[0,t_1]} |f'(t)| & 0 \leq t \leq t_1 \\ \sup_{t\in[t_1,T]} \left|\dfrac{f'(t)}{g'(t)}\right| & t_1 \leq t \leq T \end{cases}$$

$$\leq \begin{cases} \|f'\|_\infty & 0 \leq t \leq t_1 \\ \left\|\dfrac{f'(t)}{g'(t)}\right\|_\infty & t_1 \leq t \leq T. \end{cases}$$

The equilibrium points of the system are determined by solving the following system of equations

$${}_0^{PC}D_g^\alpha x_i = 0, \quad i = 1, \ldots, 4.$$

This leads to two types of equilibria. The first is the disease-free equilibrium given by:

$$\omega^0 = (d_1^{-1}\Lambda_h, 0, d_2^{-1}\Lambda_m, 0).$$

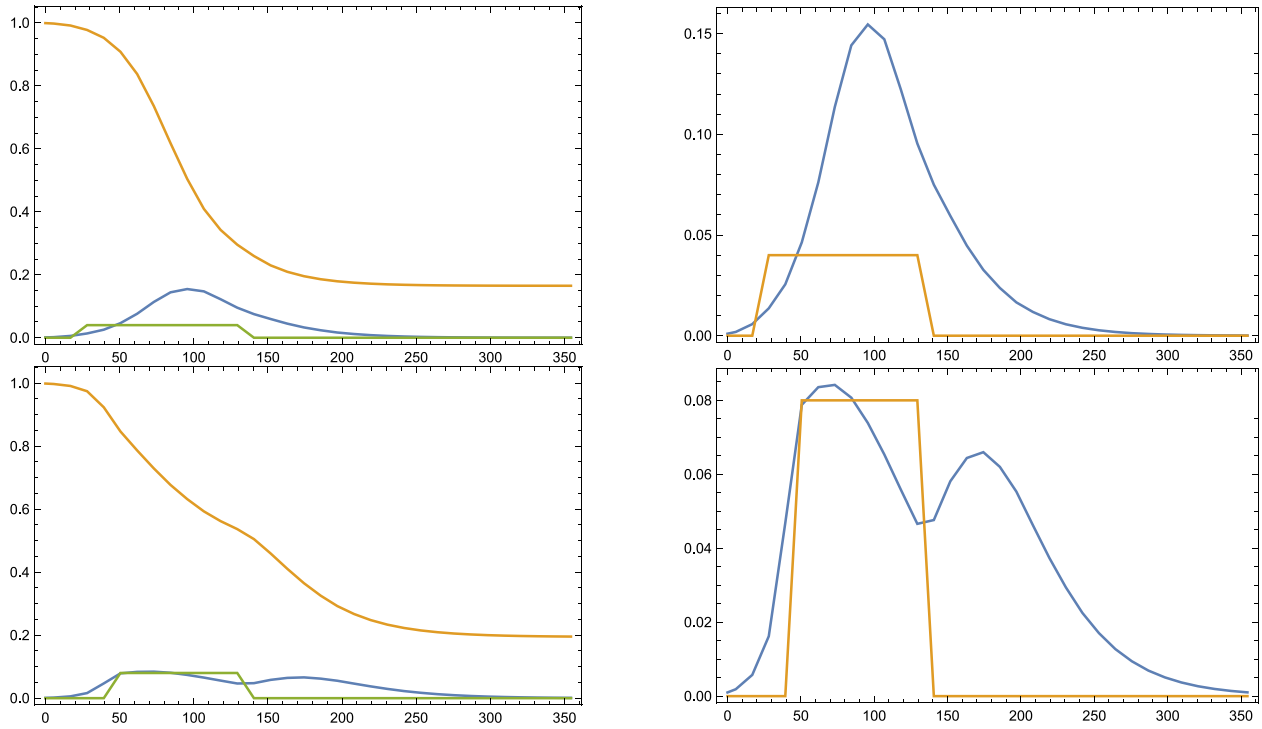

Fig. 6. Numerical solution of the SIR epidemic model with the cost functional (4) at $t_c = 360/16$ for $u_0 = 0.04$ (upper Line) and $u_0 = 0.08$ (bottom Line).

The second is the endemic equilibrium, which requires numerous algebraic steps to be evaluated. It exists only if $R_0 > 1$ but in our calculation $R_0 < 1$ as will be evaluated shortly.

In this model, the basic reproduction number R_0 is of utmost biological significance as it governs the overall dynamics of the model. It can be computed using the method introduced in [34], known as the spectral radius denoted by $\rho(M^{-1})$, applied to the matrix M^{-1}, where

$$M = \begin{bmatrix} 0 & \dfrac{d_1 d_2}{\beta_2 \gamma_2 \Lambda_m} \\ \dfrac{d_1 d_2}{\beta_1 \gamma_1 \Lambda_h} & 0 \end{bmatrix}.$$

This yields

$$R_0 = \frac{\sqrt{\beta_1 \beta_2 \gamma_1 \gamma_2 \Lambda_m \Lambda_h}}{d_1 d_2}.$$

To assess the stability of the system, we select $\alpha > 0$ and make the assumption that $R0 < 1$. Employing a Lyapunov function, we can then establish:

$$\begin{aligned} \Pi(t) &= \Xi_1 \left(x_1 - d_1^{-1} \Lambda_h \left(1 + \ln d_1^{-1} \Lambda_h x_1 \right) \right) + \Xi_2 x_2 \\ &\quad + \Xi_3 \left(x_3 - d_2^{-1} \Lambda_m \left(1 + \ln d_2^{-1} \Lambda_h x_3 \right) \right) + \Xi_4 x_4, \end{aligned} \tag{10}$$

for some positive constants $\Xi_1, i = 1, \ldots, 4$.

Now, by applying the time derivative ${}_0^{PC}D_g^{\alpha}$ to Eq. (10), we obtain:

$$\begin{aligned} {}_0^{PC}D_g^{\alpha}\Pi(t) &= \Xi_1 \left(1 - \frac{d_1^{-1}\Lambda_h}{x_1} \right) {}_0^{PC}D_g^{\alpha} x_1 + \Xi_2 \, {}_0^{PC}D_g^{\alpha} x_2 \\ &\quad + \Xi_3 \left(1 - \frac{d_2^{-1}\Lambda_m}{x_3} \right) {}_0^{PC}D_g^{\alpha} x_3 + \Xi_4 \, {}_0^{PC}D_g^{\alpha} x_4. \end{aligned}$$

Implementing the definitions of these derivatives as provided in Eq. (8), we arrive at:

$$\begin{aligned} {}_0^{PC}D_g^{\alpha}\Pi(t) &= \Xi_1 \left(1 - \frac{d_1^{-1}\Lambda_h}{x_1} \right) \left(\Lambda_h - \beta_1 \gamma_1 x_1(t) x_4(t) - d_1 x_1(t) \right) \\ &\quad + \Xi_2 (\beta_1 \gamma_1 x_1(t) x_4(t) - d_1 x_2(t)) \\ &\quad + \Xi_3 \left(1 - \frac{d_2^{-1}\Lambda_m}{x_3} \right) (\Lambda_m - \beta_2 \gamma_2 x_2(t) x_3(t) - d_2 x_3(t)) \\ &\quad + \Xi_4 (\beta_2 \gamma_2 x_2(t) x_3(t) - d_2 x_4(t)). \end{aligned}$$

Simplifying the last equation yields:

$$\begin{aligned} {}_0^{PC}D_g^{\alpha}\Pi(t) &= \beta_1 \gamma_1 (\Xi_2 - \Xi_1) x_1 x_4 + \beta_2 \gamma_2 (\Xi_4 - \Xi_3) x_2 x_3 \\ &\quad + (\Xi_1 \beta_1 \gamma_1 d_1^{-1} \Lambda_h - \Xi_4 d_2) x_4 + (\Xi_3 \beta_1 \gamma_1 d_2^{-1} \Lambda_m - \Xi_2 d_1) x_2. \end{aligned}$$

By setting

$$\Xi_1 = \beta_2 \gamma_2 d_2^{-1} \Lambda_m = \Xi_2, \Xi_3 = d_1 = \Xi_4,$$

we can simplify the equation as follows:

$${}_0^{PC}D_g^{\alpha}\Pi(t) = d_1 d_2 (R_0 - 1) x_4.$$

This implies that

$${}_0^{PC}D_g^{\alpha}\Pi(t) < 0, \ when \ R_0 - 1 < 0,$$

thereby confirming the stability of the set of unknown equations $\{x_1, x_2, x_3, x_4, \ where \ x_i \geq 0 \ for \ i = 1, \ldots, 4\}$.

Now, to simulate the Zika virus epidemic, we initialize the system with parameters sourced from [35]. These parameters include initial population counts for susceptible individuals ($x_1(0) = 400$), infected individuals ($x_2(0) = 100$), recovered individuals ($x_3(0) = 600$), and blood donors ($x_4(0) = 140$). Additionally, we incorporate values for transmission rates ($\Lambda_h = 1.2$, $\Lambda_m = 0.3$), infection rates ($\beta_1 = 0.0004$, $\beta_2 = 0.005$), recovery rates ($\gamma_1 = 0.02$, $\gamma_2 = 0.0003$), and population loss rates due to disease-related deaths ($d_1 = 0.004$, $d_2 = 0.0014$). The basic reproduction rate is estimated at $R_0 = \frac{3\sqrt{3}}{14} \approx 0.37115$. These parameters enable the numerical solution of the system of piecewise fractional differential Eqs. (8), allowing for an exploration of the Zika virus epidemic's dynamics and the evaluation of intervention strategies.

In Fig. 7, we compute the population counts $x_i(t)$ for $i = 1, 2, 3, 4$ using $\alpha = 1/2$, $t_1 = 300$, and $T = 600$. Notably, the total human population is represented by $x_h(t) = x_1(t) + x_2(t)$, where x_1 and x_2 denote the counts of susceptible and infected human individuals, respectively. Similarly, the mosquito population is the sum of susceptible (x_3) and

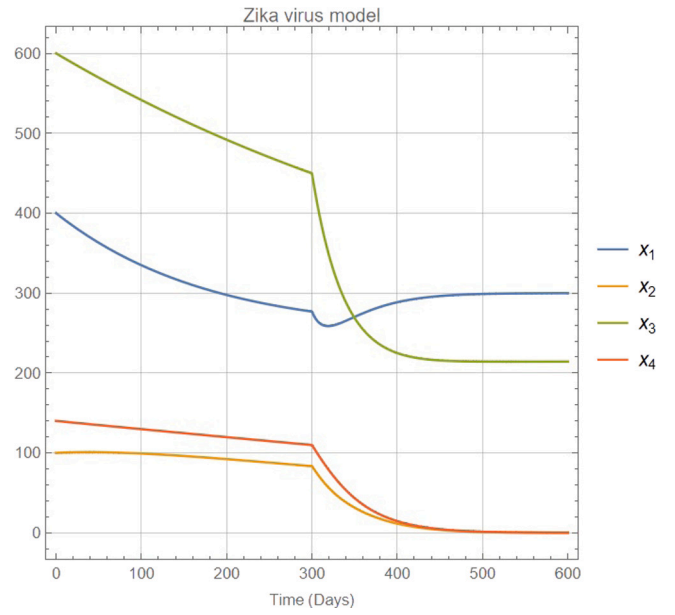

Fig. 7. Dynamics of human (x_1, x_2) and mosquito (x_3, x_4) populations in the Zika virus model using piecewise derivative.

infected (x_4) mosquitoes, given by $x_m = x_3 + x_4$. The piecewise derivative functions as a regulatory mechanism applied simultaneously to both human and mosquito populations.

3.2. Optimal SIR model

In the given system of equations, denoted as (1)–(3), we have three equations describing the dynamics of the variables $s(t)$, $x(t)$, and $y(t)$. To rewrite the system using the piecewise derivative operator ${}_0^{PG}D_g^{\alpha}$, we introduce a new system where the time derivatives are replaced by the piecewise derivative operator. The function $g(t)$ is again defined as $g(t) = \frac{t^{2-\alpha}}{2-\alpha}$, where $0 < \alpha \leq 1$.

The ${}_0^{PG}D_g^{\alpha}$ operator applied to a function $f(t)$ is defined as in , (again referring to [33]):

$$ {}_0^{PG}D_g^{\alpha} f(t) = \begin{cases} f'(t), & \text{for } 0 \leq t \leq t_1, \\ \dfrac{f'(t)}{g'(t)}, & \text{for } t_1 \leq t \leq T, \end{cases} $$

where t_1 is the transition time from the first regime to the second regime.

Additionally, we have the piecewise integral operator ${}_0^{PG}J_g f(t)$, defined as

$$ {}_0^{PG}J_g f(t) = \begin{cases} \int_0^t f(\tau)d\tau, & \text{for } 0 \leq t \leq t_1, \\ \int_{t_1}^t f(\tau)g'(\tau)d\tau, & \text{for } t_1 \leq t \leq T. \end{cases} $$

These definitions provide the necessary framework to express and analyze the given system of equations using piecewise fractional calculus operators.

By applying the piecewise integral operator ${}_0^{PG}J_t$ to the system (1)–(3), we can express the variables $s(t)$, $x(t)$, and $y(t)$ in terms of their initial values and the corresponding integrals. The resulting expressions are as follows:

For $s(t)$:

$$ s(t) = \begin{cases} s(0) - \int_0^{t_1} s(\tau)(\beta - u(\tau))x(\tau)d\tau, & \text{for } 0 \leq t \leq t_1, \\ s(t_1) - \int_{t_1}^t s(\tau)(\beta - u(\tau))x(\tau)g'(\tau)d\tau, & \text{for } t_1 \leq t \leq T. \end{cases} $$

For $x(t)$:

$$ x(t) = \begin{cases} x(0) + \int_0^{t_1} (s(\tau)(\beta - u(\tau))x(\tau) - \gamma x(\tau))\, d\tau, & \text{for } 0 \leq t \leq t_1, \\ x(t_1) + \int_{t_1}^t (s(\tau)(\beta - u(\tau))x(\tau) - \gamma x(\tau))\, g'(\tau)d\tau, & \text{for } t_1 \leq t \leq T. \end{cases} $$

For $y(t)$:

$$ y(t) = \begin{cases} y(0) + \int_0^{t_1} f(x(\tau), u(\tau))d\tau, & \text{for } 0 \leq t \leq t_1, \\ y(t_1) + \int_{t_1}^t f(x(\tau), u(\tau))g'(\tau)d\tau, & \text{for } t_1 \leq t \leq T. \end{cases} $$

These expressions provide a representation of the variables $s(t)$, $x(t)$, and $y(t)$ in terms of the initial values and the corresponding integrals involving the functions $s(\tau)$, $x(\tau)$, $u(\tau)$, $f(x(\tau), u(\tau))$, and the weight function $g'(\tau)$.

Assuming $t = t_{n+1}$ and using the initial conditions $s(0) = s_0$, $x(0) = x_0$, and $y(0) = 0$, the expressions for $s(t_{n+1})$, $x(t_{n+1})$, and $y(t_{n+1})$ can be simplified as follows:

For $s(t_{n+1})$:

$$ s(t_{n+1}) = \begin{cases} s_0 - \int_0^{t_1} s(\tau)(\beta - u(\tau))x(\tau)d\tau, & \text{for } 0 \leq t_{n+1} \leq t_1, \\ s(t_1) - \int_{t_1}^{t_{n+1}} s(\tau)(\beta - u(\tau))x(\tau)g'(\tau)d\tau, & \text{for } t_1 \leq t_{n+1} \leq T. \end{cases} $$

For $x(t_{n+1})$:

$$ x(t_{n+1}) = \begin{cases} x_0 + \int_0^{t_1} (s(\tau)(\beta - u(\tau))x(\tau) - \gamma x(\tau))\, d\tau, & \text{for } 0 \leq t_{n+1} \leq t_1, \\ x(t_1) + \int_{t_1}^{t_{n+1}} (s(\tau)(\beta - u(\tau))x(\tau) & \\ - \gamma x(\tau))\, g'(\tau)d\tau, & \text{for } t_1 \leq t_{n+1} \leq T. \end{cases} $$

For $y(t_{n+1})$:

$$ y(t_{n+1}) = \begin{cases} \int_0^{t_1} f(x(\tau), u(\tau))d\tau, & \text{for } 0 \leq t_{n+1} \leq t_1, \\ y(t_1) + \int_{t_1}^{t_{n+1}} f(x(\tau), u(\tau))g'(\tau)d\tau, & \text{for } t_1 \leq t_{n+1} \leq T. \end{cases} $$

These simplified expressions represent the values of $s(t_{n+1})$, $x(t_{n+1})$, and $y(t_{n+1})$ at time t_{n+1} in terms of the initial values s_0 and x_0, the functions $s(\tau)$, $x(\tau)$, $u(\tau)$, and $f(x(\tau), u(\tau))$, and the integration intervals based on the transition time t_1 and the final time T.

Implementing the Newton polynomial interpolation formula, we have the following:

- For $s(t_{n+1})$, if $2 \leq k \leq i$, then

$$ s(t_{n+1}) = s_0 - \sum_{k=2}^{i} \Big(\frac{5}{12} s(t_{k-2})(\beta - u(t_{k-2}))x(t_{k-2}) - \frac{4}{3} s(t_{k-1})(\beta - u(t_{k-1}))x(t_{k-1}) + \frac{23}{12} s(t_k)(\beta - u(t_k))x(t_k) \Big) $$

While if $i + 3 \leq k \leq n$:

$$ s(t_{n+1}) = s_1 - \sum_{k=i+3}^{n} \Big(\frac{5}{12}(g(t_{k-1}) - g(t_{k-2}))s(t_{k-2})(\beta - u(t_{k-2}))x(t_{k-2}) - \frac{4}{3}(g(t_k) - g(t_{k-1}))s(t_{k-1})(\beta - u(t_{k-1}))x(t_{k-1}) + \frac{23}{12}(g(t_{k+1}) - g(t_k))s(t_k)(\beta - u(t_k))x(t_k) \Big) $$

- For $x(t_{n+1})$, if $2 \leq k \leq i$, then

$$ x(t_{n+1}) = x_0 - \sum_{k=2}^{i} \Big(\frac{5}{12} \big(s(t_{k-2})(\beta - u(t_{k-2}))x(t_{k-2}) - \gamma x(t_{k-2})\big) - \frac{4}{3} \big(s(t_{k-1})(\beta - u(t_{k-1}))x(t_{k-1}) - \gamma x(t_{k-1})\big) + \frac{23}{12} \big(s(t_k)(\beta - u(t_k))x(t_k) - \gamma x(t_k)\big) \Big) $$

While if $i + 3 \leq k \leq n$:

$$ x(t_{n+1}) = x_1 - \sum_{k=i+3}^{n} \Big(\frac{5}{12}(g(t_{k-1}) - g(t_{k-2})) \big(s(t_{k-2})(\beta - u(t_{k-2})) \times x(t_{k-2}) - \gamma x(t_{k-2})\big) - \frac{4}{3}(g(t_k) - g(t_{k-1})) \big(s(t_{k-1})(\beta - u(t_{k-1}))x(t_{k-1}) - \gamma x(t_{k-1})\big) + \frac{23}{12}(g(t_{k+1}) - g(t_k)) \big(s(t_k)(\beta - u(t_k))x(t_k) - \gamma x(t_k)\big) \Big) $$

- For $y(t_{n+1})$, if $2 \le k \le i$, then

$$y(t_{n+1}) = y_0 - \sum_{k=2}^{i} \Big(\frac{5}{12} f(x(t_{k-2}), u(t_{k-2})) - \frac{4}{3} f(x(t_{k-1}), u(t_{k-1})) + \frac{23}{12} f(x(t_k), u(t_k)) \Big)$$

While if $i+3 \le k \le n$:

$$y(t_{n+1}) = y_1 - \sum_{k=i+3}^{n} \Big(\frac{5}{12}(g(t_{k-1}) - g(t_{k-2})) f(x(t_{k-2}), u(t_{k-2})) - \frac{4}{3}(g(t_k) - g(t_{k-1})) f(x(t_{k-1}), u(t_{k-1})) + \frac{23}{12}(g(t_{k+1}) - g(t_k)) f(x(t_k), u(t_k)) \Big)$$

Note that, the mathematical representation of the implementation using Newton's polynomial interpolation can be summarized to implement the system numerically in our desired software tool as follows:

Given data points:

$t = [t_0, t_1, \dots, t_n]$ (Time points)

$x = [x_0, x_1, \dots, x_n]$ (Values of x at time points)

$y = [y_0, y_1, \dots, y_n]$ (Values of y at time points)

Constants:

β, γ (given constants)

Function for $f(x, u)$:

$f(x, u)$ (definition of the function)

Function for $g'(t)$:

$g'(t)$ (definition of the function)

Function for $s(t)$ (using Newton's polynomial interpolation):

$n =$ length of t

Initialize $s_{\text{coeffs}} = [0, 0, \dots, 0]$ (coefficients of the polynomial)

Compute the divided differences:

For $j = 0$ to $n-1$:

$s_{\text{coeffs}}[j] = y[j]$

For $i = j-1$ to 0 :

$$s_{\text{coeffs}}[i+1] = \frac{s_{\text{coeffs}}[i+1] - s_{\text{coeffs}}[i]}{t[i+1] - t[i]}$$

Evaluate the polynomial at the interpolation points:

For $i = 0$ to $n-1$:

Set prod = 1

For $j = 0$ to $i-1$:

Set prod = prod $\times (t_{\text{interp}} - t[j])$

$s_{\text{interp}} = s_{\text{interp}} + s_{\text{coeffs}}[i] \times$ prod

Function for $x(t)$ (using Newton's polynomial interpolation):

$n =$ length of t

Initialize $x_{\text{coeffs}} = [0, 0, \dots, 0]$ (coefficients of the polynomial)

Compute the divided differences:

For $j = 0$ to $n-1$:

$x_{\text{coeffs}}[j] = x[j]$

For $i = j-1$ to 0 :

$$x_{\text{coeffs}}[i+1] = \frac{x_{\text{coeffs}}[i+1] - x_{\text{coeffs}}[i]}{t[i+1] - t[i]}$$

Evaluate the polynomial at the interpolation points:

For $i = 0$ to $n-1$:

Set prod = 1

For $j = 0$ to $i-1$:

Set prod = prod $\times (t_{\text{interp}} - t[j])$

$x_{\text{interp}} = x_{\text{interp}} + x_{\text{coeffs}}[i] \times$ prod.

Function for $y(t)$ (using Newton's polynomial interpolation):

$n =$ length of t

Initialize $y_{\text{coeffs}} = [0, 0, \dots, 0]$ (coefficients of the polynomial)

Compute the divided differences:

For $j = 0$ to $n-1$:

$y_{\text{coeffs}}[j] = y[j]$

For $i = j-1$ to 0 :

$$y_{\text{coeffs}}[i+1] = \frac{y_{\text{coeffs}}[i+1] - y_{\text{coeffs}}[i]}{t[i+1] - t[i]}.$$

Evaluate the polynomial at the interpolation points:

For $i = 0$ to $n-1$:

Set prod = 1

For $j = 0$ to $i-1$:

Set prod = prod $\times (t_{\text{interp}} - t[j])$

$y_{\text{interp}} = y_{\text{interp}} + y_{\text{coeffs}}[i] \times$ prod.

While both studies by Kruse [14] and Freddi [16] address optimization challenges in compartmental epidemic models, they each offer unique strengths and limitations. The research introduced in Kruse and Freddi's work presents a comprehensive system of ordinary differential equations (ODEs) that covers classical and contemporary epidemic spread models. Their methodology ensures well-posedness, positivity, and uniqueness of optimal solutions, even for nonlinear cost functionals with varied exponents. Additionally, they introduce necessary optimality conditions, deriving feedback control laws for qualitative analysis. However, their analysis is primarily confined to linear and quadratic cost functions, potentially encountering discontinuities in controls. In contrast, our paper proposes an innovative method for optimizing the control strategy of the SIR model under social distancing measures. Considering advanced numerical techniques, such as collocation with Bernoulli wavelets and Newton's iterative method, we offer a robust framework for epidemic control optimization. Our approach boasts enhanced accuracy and efficiency, especially in determining the optimal duration of lock-down periods. Furthermore, the utilization of Bernoulli wavelets opens doors to potential applications in artificial intelligence and machine learning, broadening the versatility of our approach. Therefore, while both studies significantly contribute to the field of epidemic modeling and optimization, our approach stands out for its numerical efficiency and potential applications in AI. Nonetheless, further research is necessary to fully explore the capabilities and adaptability of our methodology across diverse epidemic scenarios and population sizes. Our proposed methodology offers several advantages in understanding epidemic spread. By investigating piecewise differential and integral operators, we introduce a novel approach that enhances our comprehension of epidemic dynamics within finite time intervals. The incorporation of Bernoulli wavelets facilitates efficient simulations, enabling comprehensive analyses of epidemic behavior under various control strategies, including social distancing measures. However, a potential challenge of our approach lies in the complexity associated with implementing piecewise derivatives, necessitating an advanced mathematical expertise as discussed in [21]. Additionally, further research is needed to assess the scalability and robustness of our methodology across different epidemic scenarios and population sizes.

4. Conclusion

Our investigation represents a big step forward in improving how we control diseases, especially during times when we need to keep our distance from each other. With the current global health crisis, it is crucial to come up with effective plans. Mathematical tools like the susceptible–infected–recovered (SIR) model give us important information about how diseases spread, helping leaders make the right decisions. Our new approach offers a fresh way to make the SIR model work better within specific timeframes. Using a collocation with Bernoulli wavelets, we have looked closely at real-life disease situations and figured out the best times for lockdowns. This method is different from the usual ones, but it is more accurate and efficient in controlling diseases. While other studies have tried different ways to solve problems with the SIR model, our work stands out because we used Bernoulli wavelets in a new and creative way. These wavelets could also be useful for future work in artificial intelligence (AI) and machine learning. Our approach opens up new ways to understand and improve how we control diseases. Overall, our research shows the importance of teamwork and new ways of thinking in dealing with big global problems. By combining advanced math techniques with insights from studying diseases, we can do a better job of keeping people healthy in a world that is always changing.

CRediT authorship contribution statement

Mutaz Mohammad: Validation, Visualization, Writing – review & editing, Formal analysis, Investigation, Methodology, Project administration, Software, Supervision. **Mohyeedden Sweidan:** Formal analysis, Investigation, Methodology. **Alexander Trounev:** Data curation, Resources, Software, Writing – original draft.

Declaration of competing interest

The authors declare that they have no known competing financial interests or personal relationships that could have appeared to influence the work reported in this paper.

Acknowledgments

The first and second authors acknowledge the support of Zayed University Research Office, the Provost's Research Fellowship Award (PRFA) under grant number R22154, and Concord University for their assistance in concluding this research.

References

[1] F. Brauer, C. Castillo-Chavez, Mathematical Models in Population Biology and Epidemiology, Springer Science, Berlin, 2010.
[2] W.O. Kermack, A.G. McKendrick, A contribution to the mathematical theory of epidemics, Proc. R. Soc. Lond. Ser. A Math. Phys. Eng. Sci. 115 (1927) 700.
[3] W.O. Kermack, A.G. McKendrick, A contribution to the mathematical theory of epidemics, Proc. R. Soc. Lond. Ser. A Math. Phys. Eng. Sci. 115 (772) (1927) 700–721.
[4] H. Jafari, P. Goswami, R.S. Dubey, S. Sharma, A. Chaudhary, Fractional SIZR model of zombie infection, Int. J. Math. Comput. Exp. Eng. 9 (1) 91–104, http://dx.doi.org/10.2478/ijmce-2023-0007.
[5] R. Singh, J. Mishra, V.K. Gupta, Dynamical analysis of a tumor growth model under the effect of fractal fractional Caputo–Fabrizio derivative, Int. J. Math. Comput. Exp. Eng. 9 (2) 115–126, http://dx.doi.org/10.2478/ijmce-2023-0009.
[6] N.N. Sene, Analytical solutions of hristov diffusion equations with non-singular fractional derivatives, Chaos 29 (2) (2019) http://dx.doi.org/10.1063/1.5082645, Article 023112.
[7] A. Omame, N. Sene, I. Nometa, C.I. Nwakanma, E.U. Nwafor, N.O. Iheonu, D. Okuonghae, Analysis of COVID-19 and comorbidity co-infection model with optimal control, 2021, http://dx.doi.org/10.1002/oca.2748, First published: 02 2021.
[8] Venkatesan Govindaraj, Raju K. George, Controllability of fractional dynamical systems: A functional analytic approach, Math. Control Relat. Fields 7 (4) (2017) 537–562, http://dx.doi.org/10.3934/mcrf.2017020.
[9] Venkatesan Govindaraj, Raju K. George, Functional approach to observability and controllability of linear fractional dynamical systems, Int. J. Dyn. Control 5 (2) (2017) 111–129, http://dx.doi.org/10.1080/1726037X.2017.1390191.
[10] R. Poovarasan, Pushpendra Kumar, Kottakkaran Sooppy Nisar, V. Govindaraj, The existence, uniqueness, and stability analyses of the generalized Caputo-type fractional boundary value problems, Mathematics 8 (7) (2023) 16757–16772, http://dx.doi.org/10.3934/math.2023857.
[11] R. Poovarasan, P. Kumar, V. Govindaraj, et al., The existence, uniqueness, and stability results for a nonlinear coupled system using ψ-Caputo fractional derivatives, Bound. Value Probl. 2023 (75) (2023) http://dx.doi.org/10.1186/s13661-023-01769-4.
[12] R. Poovarasan, P. Kumar, S.M. Sivalingam, et al., Some novel analyses of the Caputo-type singular three-point fractional boundary value problems, J. Anal. 32 (2024) 637–658, http://dx.doi.org/10.1007/s41478-023-00638-8.
[13] L. Bolzonia, E. Bonacinib, C. Soresinac, M. Groppi, Time-optimal control strategies in SIR epidemic models, Math. Biosci. 292 (2017) 86–96.
[14] T. Kruse, P. Strack, Optimal Control of an Epidemic Through Social Distancing, Yale University, New Haven, 2020.
[15] E. Hansen, T. Day, Optimal control of epidemics with limited resources, J. Math. Biol. 62 (3) (2011) 423–451.
[16] L. Freddi, Optimal control of the transmission rate in compartmental epidemics, Math. Control Relat. Fields 11 (3) (2021) 1–23.
[17] J. Nocedal, S.J. Wright, Numerical Optimization, pringer-Verlag, New York, 1999.
[18] J.T. Bets, Practical methods for optimal control using nonlinear programming, Soc. Ind. Appl. Math. (SIAM) (2001) Philadelphia.
[19] F. Bonnans, P. Martinon, D. Giorgi, V. Grelard, S. Maindrault, O. Tissot, J. Liu, The optimal control solver BOCOP 2.2.0 - User Guide, 2019, https://www.bocop.org, Accessed 15 2021.
[20] E. Keshavarz, Y. Ordokhani, M. Razzaghi, The Bernoulli wavelets operational matrix of integration and its applications for the solution of linear and nonlinear problems in calculus of variations, Appl. Math. Comput. (ISSN: 0096-3003) 351 (2019) 83–98, http://dx.doi.org/10.1016/j.amc.2018.12.032.
[21] M. Mohammad, A. Trounev, C. Carlo, Stress state and waves in the lithospheric plate simulation: A 3rd generation AI architecture, Results Phys. 53 (2023) http://dx.doi.org/10.1016/j.rinp.2023.106938.
[22] M. Mohammad, A. Trounev, On the dynamical modeling of Covid-19 involving Atangana-Baleanu fractional derivative and based on Daubechies framelet simulations, Chaos Solitons Fractals 140 (2020) http://dx.doi.org/10.1016/j.chaos.2020.110171.
[23] M. Mohammad, A. Trounev, C. Cattani, The dynamics of COVID-19 in the UAE based on fractional derivative modeling using Riesz wavelets simulation, Adv. Differ. Equ. 2021 (2021) 115, http://dx.doi.org/10.1186/s13662-021-03262-7.
[24] M.H.T. Alshbool, M. Mohammad, O. Isik, I. Hashim, Fractional Bernstein operational matrices for solving integro-differential equations involved by Caputo fractional derivative, Res. Appl. Math. 14 (2022) http://dx.doi.org/10.1016/j.rinam.2022.100258.
[25] B. Ghanbari, On approximate solutions for a fractional prey–predator model involving the Atangana–Baleanu derivative, Adv. Difference Equ. 2020 (679) http://dx.doi.org/10.1186/s13662-020-03140-8.
[26] B. Ghanbari, On the modeling of the interaction between tumor growth and the immune system using some new fractional and fractional-fractal operators, Adv. Difference Equ. 2020 (585) (2020).
[27] B. Ghanbari, A fractional system of delay differential equation with nonsingular kernels in modeling hand-foot-mouth disease, Adv. Differ. Equ. 2020 (2020) 536, http://dx.doi.org/10.1186/s13662-020-02993-3.
[28] Behzad Ghanbari, On novel nondifferentiable exact solutions to local fractional Gardner's equation using an effective technique, 2020, http://dx.doi.org/10.1002/mma.7060, First published: 25 November 2020.
[29] Behzad Ghanbari, On approximate solutions for a fractional prey–predator model involving the Atangana–Baleanu derivative, Adv. Difference Equ. 2020 (679) http://dx.doi.org/10.1002/mma.7302.
[30] Behzad Ghanbari, A new model for investigating the transmission of infectious diseases in a prey-predator system using a non-singular fractional derivative, 2021, http://dx.doi.org/10.1002/mma.7412, *First published: 16 2021*.
[31] Behzad Ghanbari, Chaotic behaviors of the prevalence of an infectious disease in a prey and predator system using fractional derivatives, 2021, http://dx.doi.org/10.1002/mma.7386, *First published: 06 2021*.
[32] Behzad Ghanbari, Abdon Atangana, Some new edge detecting techniques based on fractional derivatives with non-local and non-singular kernels, Adv. Difference Equ. 2020 (435).
[33] A. Atangana, A.S. Iğret, New concept in calculus: Piecewise differential and integral operators, Chaos Solitons Fractals 145, 110638, http://dx.doi.org/10.1016/j.chaos.2020.110638.
[34] P. van den Driessche, J. Watmough, Reproduction numbers and sub-threshold endemic equilibria for compartmental models of disease transmission, Bellman Prize Math. Biosci. 180 (2002) 29–48.
[35] A.K. Muhammad, U. Saif, F. Muhammad, The dynamics of zika virus with Caputo fractional derivative, AIMS Math. 4 (2019) 134–146, http://dx.doi.org/10.3934/Math.2019.1.134.